Microwave spectroscopy of a Cooper-pair transistor coupled to a lumped-element resonator

Matthew T. Bell, Lev B. Ioffe, and Michael E. Gershenson
Department of Physics and Astronomy, Rutgers University, 136 Frelinghuysen Rd., Piscataway, New Jersey 08854, USA
(Received 11 November 2011; revised manuscript received 13 August 2012; published 11 October 2012)

We have studied the microwave response of a single Cooper-pair transistor (CPT) coupled to a lumped-element microwave resonator. The resonance frequency of this circuit, f_r, was measured as a function of the charge n_g induced on the CPT island by the gate electrode and the phase difference across the CPT, ϕ_B, which was controlled by the magnetic flux in the superconducting loop containing the CPT. The observed $f_r(n_g,\phi_B)$ dependencies reflect the variations of the CPT Josephson inductance with n_g and ϕ_B as well as the CPT excitation when the microwaves induce transitions between different quantum states of the CPT. The results are in excellent agreement with our simulations based on the numerical diagonalization of the circuit Hamiltonian. This agreement over the whole range of n_g and ϕ_B is unexpected, because the relevant energies vary widely, from 0.1 to 3 K. The sensitivity of the CPT as an electrometer is peaked when the CPT excitation level approaches that of the microwave resonator.

DOI: 10.1103/PhysRevB.86.144512 PACS number(s): 85.25.Cp

I. INTRODUCTION

The Cooper-pair transistor (CPT) is a three-terminal device that consists of a mesoscopic superconducting island connected to two leads by two Josephson tunnel junctions (JJs) (see, e.g., Refs. 1 and 2 and references therein). The behavior of this device is controlled by two energies: the charging energy per junction, $E_C \equiv e^2/2C_J$ (C_J is the capacitance of a single tunnel junction), and the Josephson coupling energy E_J. The energies E_C and E_J could be made of the same order of magnitude by reducing the tunnel junction in-plane dimensions (typically, down to 100–200 nm for Al-AlO_x-Al junctions). The energies of quantum states of the CPT are $2e$ periodic in a continuous charge $n_g = C_g V_g/e$ induced on the island by a capacitively coupled gate electrode. Here, C_g is the capacitance of the capacitor formed by the island and the gate electrode, V_g is the voltage applied to this capacitor. The sensitivity of the CPT characteristics to the induced charge makes this device a very sensitive electrometer which, in particular, can operate in a low-dissipation dispersive mode.[3–5] The interplay between the Josephson effect and Coulomb blockade leads to a quantum superposition of charge states in the CPT, which forms the basis for quantum computing with superconducting charge qubits.[6–8] Since the first demonstration of the coherent superposition of states in the CPT more than a decade ago, the CPT has been used as a test bed for many novel experimental techniques employed in the research on superconducting qubits.

The microwave experiments with CPTs can be broken down into two main categories. In the first type of measurements, the CPT remains in its ground state because of a large mismatch between the probe signal frequency and the excitation frequencies of the CPT. During this adiabatic operation, the CPT can be described by its effective microwave impedance. This impedance, depending on the parameters of the Josephson junctions and the coupling of the CPT to the readout circuit, could be predominantly inductive (the Josephson inductance, the second derivative of the CPT energy in phase[9]) or capacitive (the quantum capacitance, the second derivative of the CPT energy in charge[10–12]). If the CPT is coupled to a resonator and their levels are close in energy, the entanglement of the CPT and resonator states affects the impedance of this circuit even if the microwaves do not induce transitions between the CPT states. In the latter case, the impedance-based description of the CPT is insufficient, and the solution of the quantum Hamiltonian of the system "CPT + read-out circuit" is required. In the second type of measurements, the microwaves induce transitions between different quantum states of the CPT. This, in particular, enables the preparation and manipulation of coherent superpositions of the ground and excited states in the quantum-computing-related applications of the CPT.

In this paper, we present the microwave spectroscopic study of a CPT that probes both the ground state and excited states of the CPT over wide ranges of the charge n_g and the phase difference across the CPT, ϕ_B. The phase was controlled by the magnetic flux in the superconducting loop containing the CPT. The CPT microwave response was analyzed by measuring the resonance frequency f_r of the combined circuit containing a lumped-element microwave resonator (referred below as an LC resonator) and a CPT. When the detuning between the LC-resonator frequency and the excitation frequencies of the CPT was large, the dependence $f_r(n_g,\phi_B)$ mostly reflected the variations of the CPT Josephson inductance with n_g and ϕ_B. On the other hand, an avoided crossing of the CPT and LC-resonator levels was clearly observed when the CPT excitation frequency was tuned to the LC-resonator frequency by varying n_g and ϕ_B. The overall dependence $f_r(n_g,\phi_B)$ is in excellent agreement with the simulations based on the numerical diagonalization of the circuit Hamiltonian. This agreement illustrates the accuracy of our numerical simulations that can be applied to more complicated, multijunction circuits in the quantum regime, including the superconducting circuits envisioned as protected superconducting qubits.[13,14]

The paper is organized as follows. In Sec. II, we describe the samples and measurement techniques. The details of numerical simulations of this circuit are provided in Sec. III. The experimental results are discussed and compared with numerical simulations in Sec. IV.

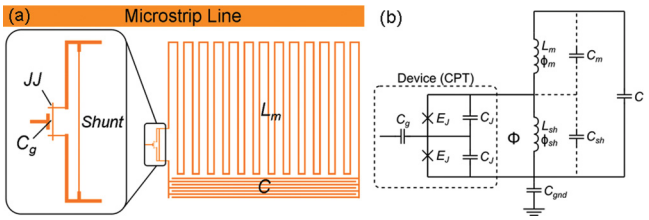

FIG. 1. (Color online) Schematics of the "CPT + LC resonator" circuit. (a) The on-chip circuit layout. The superconducting shunting wire ("shunt") serves two purposes: it reduces the coupling of the CPT to the LC resonator (and, thus, reduces external noises), and it forms, in combination with the CPT, a superconducting loop. The magnetic flux in the loop controls the phase difference across the CPT. (b) The circuit diagram used for modeling in Sec. III.

II. DEVICE FABRICATION AND MEASURING TECHNIQUES

A. Circuit design and device fabrication

The schematics of the tested circuit is shown in Fig. 1. The CPT is inductively coupled via a narrow Al wire ("shunt") to a lumped-element LC resonator. The LC resonator, which is strongly coupled to the microstrip line, consists of a meandered 2-μm-wide Al wire with $L_m = 5$ nH and an interdigitated capacitor (2-μm-wide fingers with 2 μm spacing between them) with $C = 100$ fF. The typical values of the internal and loaded quality factors for these LC resonators (not coupled to the CPT) were 50 000 and 20 000, respectively. High Q values enable sensitive measurements of small changes in the microwave impedance of the tested device induced by the variations of n_g and ϕ_B. Outside of its bandwidth, the LC resonator efficiently decouples the CPT from external noises. An additional protection of the CPT from external noises is provided by the shunt: the kinetic inductance of this superconducting wire, $L_{\rm sh} = 0.5$ nH, is more than ten times smaller than the effective Josephson inductance of the CPT, and this significantly reduces the phase fluctuations across the CPT. The LC resonator is inductively coupled to a two-port Al microstrip line with a 50-Ω wave impedance. The gate electrode of the CPT is coupled to the central island of the CPT through a capacitor $C_g = 0.2$ fF. A similar circuit (a CPT inserted in a superconducting loop which is inductively coupled to an LC resonator tank circuit) was proposed by Zorin,[15] and realized in experiments.[16,17] Note that the entanglement between the CPT and LC resonator levels was not observed in these works due to a relatively low resonance frequency of the tank circuit (approximately ten times smaller than in the present experiment).

The Cooper-pair transistor, the lumped-element LC resonator, and the microstrip line were fabricated within the same vacuum cycle using multiangle electron-beam deposition of Al films through a nanoscale lift-off mask (for details, see Ref. 14). The central island of the Cooper-pair transistor was always deposited during the first Al deposition, and its thickness (20 nm) was smaller than that of the leads (60 nm); this is important for preventing quasiparticle poisoning.[18] The spread of the resistances for the nominally identical JJs with an area of 0.15×0.15 μm^2 did not exceed 10%. More than ten devices with $E_J/E_C = 1.5$–3 have been studied and the results have been successfully fitted with the numerical simulations; below we discuss several representative samples.

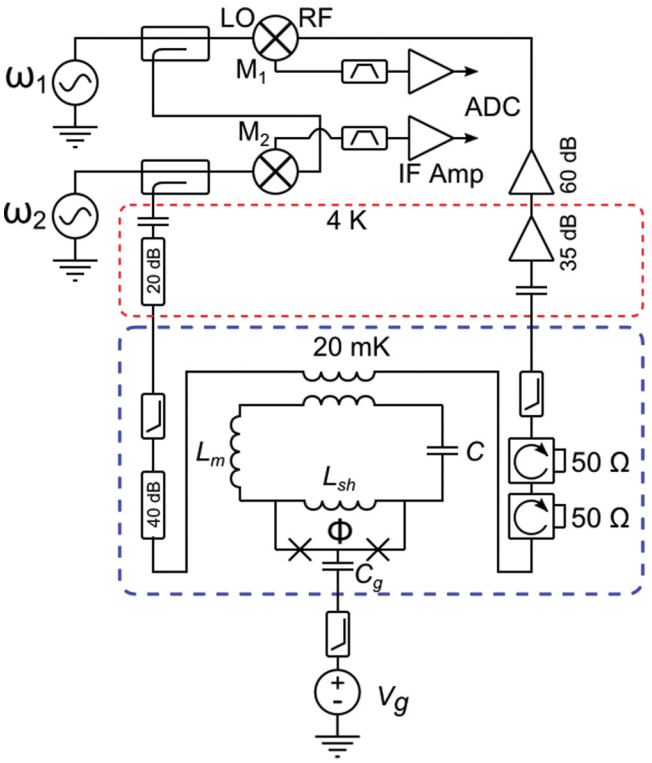

FIG. 2. (Color online) Simplified circuit diagram of the measurement setup. The microwaves at ω_2 are transmitted through the microstrip line coupled to the "LC resonator + CPT" circuit. This signal is amplified, mixed down to an intermediate frequency $\omega_1 - \omega_2$, and digitized by a fast digitizer (ADC). The second channel of the ADC is used to digitize the signal from an additional mixer (M2), which provided the reference phase φ_0 (see the text). The gate voltage V_g is applied to the capacitor C_g using a heavily filtered DC line.

B. Measurement technique

The microwave response of the coupled system "CPT + LC resonator" was probed by measuring the amplitude and phase of the microwaves traveling along a microstrip line coupled to the LC resonator. Figure 2 shows a simplified schematic of the microwave circuit, which is similar to the one used in Ref. 19. The cold attenuators and low-pass filters in the input microwave line prevented leakage of thermal radiation into the LC resonator. On the output line, a combination of low-pass filters and two cryogenic Pamtech isolators (approximately 18 dB isolation between 3 and 12 GHz) anchored to the mixing chamber were used to attenuate the 5-K noise temperature from the cryogenic amplifier. The DC line for the gate voltage control was heavily filtered with a combination of room temperature LC and low-temperature RC filters, followed by a stainless steel powder filter, and a 1:1000 voltage divider.

The probe signal at frequency ω_2, generated by a microwave synthesizer, was coupled to the cryostat input line through a 16 dB coupler. This signal, after passing the sample, was amplified by a cryogenic HEMT amplifier (Caltech CITCRYO 1-12, 35 dB gain between 1 and 12 GHz)

and two 30 dB room-temperature amplifiers. The amplified signal was mixed by mixer M1 with the local oscillator signal at frequency ω_1, generated by another synthesizer. The intermediate-frequency signal $a(t) = a\sin(\Omega t + \varphi) + \text{noise}(t)$ at $\Omega \equiv (\omega_1 - \omega_2)/2\pi = 30$ MHz was digitized by a 1 GS/s digitizing card (AlazarTech ATS9870). The signal was digitally multiplied by $\sin(\Omega t)$ and $\cos(\Omega t)$, averaged over many (typically, 10^6) periods, and its amplitude a (proportional to the microwave amplitude S_{21}) and phase φ were extracted as $a = \sqrt{\langle a^2(t)\sin^2\Omega t + a^2(t)\cos^2\Omega t\rangle}$ and $\varphi = \arctan[\langle a^2(t)\sin^2\Omega t\rangle/\langle a^2(t)\cos^2\Omega t\rangle]$, respectively (here, $\langle ...\rangle$ stands for the time averaging over integer number of periods). The value of φ randomly changes when both ω_1 and ω_2 are varied. To eliminate these random variations, we have also measured the phase φ_0 of the reference signal provided by mixer M2 and digitized by the second channel of the ADC. The phase difference $\varphi - \varphi_0$ at fixed n_g and ϕ_B depends only on the electric length difference between the microwave lines inside and outside of the cryostat, and is immune to the phase jitter between the two synthesizers. The measurements have been performed at microwave excitation level down to -140 dBm which corresponded to sub-single-photon population of the tank circuit.

The sample was mounted inside an rf-tight copper box that provided the ground plane for the microstrip line and LC resonator. This box was housed inside another rf-tight copper box in order to attenuate stray infrared photons.[20] This nested-box construction was anchored to the mixing chamber of a cryogen-free dilution refrigerator with a base temperature of 20 mK.

III. MODEL HAMILTONIAN AND NUMERICAL SIMULATIONS

We begin with the discussion of the theoretical model of a more general circuit which contains an arbitrary Josephson device coupled via a superconducting "shunt" to a microwave LC resonator. The generalized circuit shown in Fig. 1(b) includes two loops: the long meandering wire, the shunt, and a large capacitor C form one loop (referred below as the LC-resonator loop), and the device and the shunt form another loop (referred as the device loop). The only limitation on the device parameters is that all characteristic energies of the device are much smaller than the effective inductive energies of all superconducting wires in the device loop, $E_{L_i} = \hbar^2/[(2e)^2 L_i]$. The resonance frequency of the LC resonator might be of the same order or even very close to the device excitation energies, which would lead to the level repulsion. To simplify the notations, we shall use below the units $\hbar = 2e = 1$ (e.g., in these units $V = d\phi/dt$) and restore the physical units at the end, where we apply this model to the specific case of a device that consists of two Josephson junctions and one superconducting island, i.e., the CPT.

The generalized circuit is characterized by the inductance of the meander (shunt), L_m ($L_{\rm sh}$), and the phase difference across this element, ϕ_m ($\phi_{\rm sh}$). The difference between the device phase ϕ_0 and the shunt phase $\phi_{\rm sh}$ is due to the time-independent magnetic flux Φ in the device loop: $\phi_0 - \phi_{\rm sh} = \phi_B$, where $\phi_B = 2\pi\Phi/\Phi_0$, Φ_0 is the flux quantum. The voltage differences across the meander, device, and shunt are V_m, V_0, and $V_{\rm sh}$, respectively ($V_0 = V_{\rm sh}$). The whole circuit is described by the Lagrangian

$$\mathcal{L} = T_{\rm sh}(V_{\rm sh}) + T_m(V_m) + \frac{C}{2}(V_{\rm sh} + V_m)^2 - \frac{1}{2}E_{\rm sh}\phi_{\rm sh}^2 - \frac{1}{2}E_m{\phi_m}^2 + \mathcal{L}_D(\phi_0, V_0). \quad (1)$$

Here, $T_m(V_m)$ [$T_{\rm sh}(V_{\rm sh})$] is the generalized kinetic energy part of the response of the meander (shunt), E_m ($E_{\rm sh}$) is the inductive energy of the meander (shunt), and $\mathcal{L}_D(\phi_0, V_0)$ is the device Lagrangian which also depends on the internal degrees of freedom (phases) of the device. In the BCS theory, the energy of a superconducting wire remains practically equal to its value at $\omega = 0$, E_L, at all frequencies $\omega \lesssim \Delta$, where Δ is the superconducting gap. Its small frequency-dependent part is a function of the dimensionless parameter V/Δ:

$$T = E_L f(V/\Delta) = (1/16)(V/\Delta)^2 + O[(V/\Delta)^4].$$

This equation implies that at low frequencies, the wire impedance acquires, in addition to the kinetic inductance, a small capacitive component $C' = E_L/(8\Delta^2)$ [these capacitances are shown in Fig. 1(b) by dashed lines]. At relevant frequencies (approximately 10 GHz), the capacitive part of the wire impedance is 100 times greater than its inductive part. However, we cannot ignore this capacitance because it determines the frequency of the second mode in the LC resonator loop (see below).

We shall assume that the device Lagrangian is given by the sum of the Josephson and electrostatic energies:

$$\mathcal{L}_D(\phi_0, V_0) = \frac{1}{2}\sum_{i,j} C_{ij}V_iV_j + \sum_{i,j} J_{ij}\cos(\phi_i - \phi_j - \Phi_{ij}). \quad (2)$$

Here, phases ϕ_i and corresponding potentials V_i describe both the internal degrees of freedom of the device and the shunt phase, C_{ij} and J_{ij} are the matrices of capacitive and Josephson couplings between superconducting wires, respectively.

Because the potential energy of the shunt is much greater than that of the device, the effect of the device on the LC-resonator loop can be treated as a small perturbation. In the absence of the device, the LC-resonator loop has two modes: the harmonic oscillation of the total phase $\phi_{\rm sh} + \phi_m$ with frequency $\omega_0 = \sqrt{1/L'C}$, where $L' = E_m^{-1} + E_{\rm sh}^{-1}$, $E_{\rm sh}\phi_{\rm sh} = E_m\phi_m$, and the second mode with $\phi_m + \phi_{\rm sh} \approx 0$. Because the large capacitance C does not participate in the second mode, the frequency of this mode, ω_p, is determined by the superconducting gap, the only energy scale in this case: $\omega_p \sim \Delta$. We shall assume that $\Delta \gg \omega_0$ so both real and virtual excitations of this mode can be neglected as well as the contribution of the capacitances $C'_{\rm sh}$ and C'_m to the effective capacitance C of the first mode. Note, however, that the virtual processes involving the second mode are small only in ω_0/Δ and might not be completely negligible in a realistic situation. Another important constraint on the experimental parameters comes from the condition that the zero-point phase fluctuations of the second mode have to be small: $\langle\delta\phi^2\rangle = \omega_p/2E_{\rm sh} = (\omega_p/\Delta)R_{\rm sh}/R_Q$, where $R_{\rm sh}$ is the shunt resistance in the normal state and $R_Q = h/e^2$ is the resistance quantum. This translates into a bound on the weakness of the

LC resonator: device coupling. In the case of the device studied in this work, these fluctuations were $\langle\delta\phi^2\rangle \approx 0.05 \ll 1$. If the effects of the second mode can be neglected, there is only one relevant degree of freedom, the phase across the device ϕ_0. The effective Lagrangian that describes the remaining degrees of freedom is reduced to

$$\mathcal{L}_{\rm eff} = \frac{C_L}{2}V_0^2 - \frac{1}{2}E_L(\phi_0-\phi_B)^2 + \mathcal{L}_D(\phi_0, V_0) \tag{3}$$

with $C_L = C(1+E_{\rm sh}/E_m)^2$ and

$$E_L = E_{\rm sh}(1+E_{\rm sh}/E_m). \tag{4}$$

Fluctuations of the phase ϕ_0 in the low-energy states of the oscillator mode are very small:

$$\langle(\phi_0-\phi_B)^2\rangle = A^2(2n+1) \ll 1, \quad A^2 = \frac{\omega_0}{2E_L},$$

where n is the quantum number of the oscillator states. This allows one to replace the solution of the full problem by the solution of the simplified model in which we expand the interaction term in small phase fluctuations.

It will be more convenient to use the Hamiltonian formalism in which the conjugated degrees of freedom are phases and charges (e.g., the charge q_0 is conjugated to the phase ϕ_0). The total Hamiltonian is the sum of three parts, the Hamiltonians of the LC resonator (H_R), device (H_D), and interaction between them ($H_{\rm int}$) :

$$H_R = \frac{\omega_0^2}{2E_L}q_0^2 + \frac{1}{2}E_L(\phi_0-\phi_B)^2, \tag{5}$$

$$H_{\rm int} = C_L^{-1}\sum_{i,j>0} q_0 C_{0j}C_{ji}^{-1}(\mathbf{q}_i - n_i) - \sum_i J_{i0}\cos(\phi_0-\phi_j-\Phi_{0i}), \tag{6}$$

$$H_D = \frac{1}{2}\sum_{ij>0}(\mathbf{q_i}-n_i)C_{ij}^{-1}(\mathbf{q}_j-n_j) - \frac{1}{2}\sum_{ij>0}J_{ij}\cos(\phi_i-\phi_j-\Phi_{ij}). \tag{7}$$

Here, n_i are the offset charges on superconducting islands, Φ_{ij} are phases induced by the magnetic flux Φ, $\sum\Phi_{ij} = 2\pi\Phi/\Phi_0$. The coupling to the inductor charge fluctuations contains the inverse of the capacitance matrix ($\sim C_L^{-1}$) and thus is very small. Thus even though the charge fluctuations across the shunt are not small,

$$\langle {q_0}^2\rangle = \frac{1}{4A^2}(2n+1) \gg 1,$$

their effect on the coupling can be treated perturbatively. In the leading order in the interaction, we need to keep only two types of terms. The first type is quadratic in phase ϕ_0 and diagonal in the basis of resonator states. The second type is linear in ϕ_0 and off diagonal in this basis. The quadratic terms in the inductor charge are absent, so the charge coupling appears only due to the off diagonal terms that are linear in q_0. The Hamiltonian equivalent to Eq. (3) becomes

$$H_{\rm eff} = (\omega_0 + 2A^2\Xi)(a^\dagger a + 1/2) + \left(A\mathbf{J} + \frac{1}{4A}\mathbf{Q}\right)a + \text{H.c.} \tag{8}$$

Here, $a\dagger$ (a) is the creation (annihilation) operator for the harmonic oscillations of the mode ϕ_0 of the circuit, $\mathbf{J}$, $\mathbf{Q}$, and Ξ are operators acting on the device whose forms are obtained by expanding the interaction Hamiltonian:

$$\mathbf{J} = \left.\frac{dL}{d\phi_0}\right|_{\phi_0=0} = -\sum_i J_{i0}\sin(\phi_j+\Phi_{0i}), \tag{9}$$

$$\mathbf{Q} = C_L^{-1}\sum_{i,j>0} C_{0j}C_{ji}^{-1}(\mathbf{q}_i - n_i), \tag{10}$$

$$\Xi = \frac{1}{2}\left.\frac{d^2L}{d\phi_0^2}\right|_{\phi_0=0} = \frac{1}{2}\sum_i J_{i0}\cos(\phi_j+\Phi_{0i}). \tag{11}$$

We now estimate the scale of the frequency deviations induced by these perturbations. In the natural units of the LC resonator frequency ω_0, the scales of the perturbing operators are $A\mathbf{J}/\omega_0 \sim E_J/\sqrt{\omega_0 E_L}$, $A^{-1}\mathbf{Q}/\omega_0 \sim \sqrt{\omega_0/E_L}$, and $A^2\Xi/\omega_0 \sim E_J/E_L$. The operator Ξ is diagonal in the oscillator states, so it directly results in the frequency shift $\delta\omega_\Xi/\omega_0 \sim E_J/E_L$. Because the nondiagonal elements affect the level of the LC resonator only in the second order of the perturbation theory, the effect of the $\mathbf{J}$ and $\mathbf{Q}$ operators depends on the gap between the levels in the combined device + LC resonator circuit. Far away from the full frustration and charge degeneracy point ($\phi_B = \pi$, $n_g = 0.5$), the device is characterized by large $E_J \gg \omega_0$ and the energy levels are separated by large gaps, so the smallest gap is due to the LC resonator: $\delta E = \omega_0$. In this case, the frequency shifts are $\delta\omega_J/\omega_0 \sim E_J^2/(\omega_0 E_L)$ and $\delta\omega_Q/\omega_0 \sim \omega_0/E_L$ respectively, which implies $\delta\omega_J \gg \delta\omega_\Xi \gg \delta\omega_Q$. The effect induced by the phase and charge coupling grows when the gap between the levels coupled by these operators becomes small, but the phase coupling remains larger than the charge coupling for the devices with $E_J \gg \omega_0$. This increase of the frequency shift occurs, for instance, when the device level crosses the first LC resonator level.

We now write down the explicit equations for the Cooper pair box. In this case, the internal degrees of freedom are limited to one phase ϕ_1 and the conjugated charge q_1. Assuming equal capacitances and Josephson energies of the CPT junctions, we have

$$H_{\rm CPT} = 4E_c(q_1-n_g)^2 - E_J[\cos(\phi_1)+\cos(\phi_1+\phi_B)], \tag{12}$$

$$\mathbf{J} = -E_J\sin(\phi_1+\phi_B), \tag{13}$$

$$\mathbf{Q} = \frac{2C}{C_L}E_c(q_1-n_g), \tag{14}$$

$$\Xi = \tfrac{1}{2}E_J\cos(\phi_1+\phi_B). \tag{15}$$

Here, we restored the physical energy units $E_c = e^2/2C_J$. For practical computations, it is sufficient to retain the first few levels of the LC resonator ($a^\dagger a \leqslant n_{\max} = 3$) and some number n_Q of the charging states. The Hamiltonian (8) becomes $3n_Q \times 3n_Q$ matrix. Because the wave function of the charge decreases exponentially at large charges, $\Psi(q) \sim \exp(-\sqrt{E_c/E_J}q^2)$, it is sufficient to consider $n_Q \sim 10$ for accurate computations. The straightforward numerical

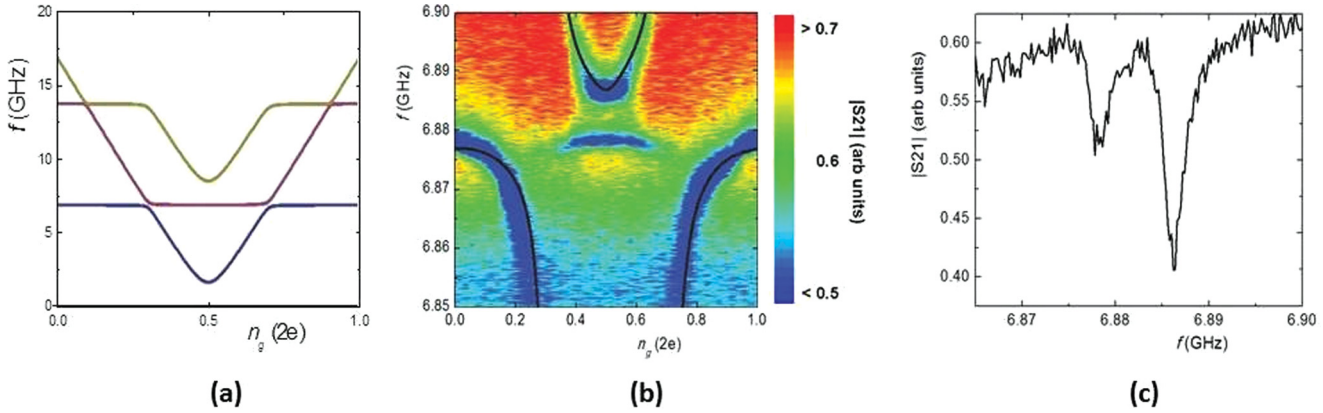

FIG. 3. (Color online) (a) Frequencies of three lowest-energy levels for the coupled system "CPT + LC resonator" plotted as a function of n_g at a constant phase $\phi_B = 0.97\pi$. The model parameters are $E_J = h \times 17.2$ GHz, $E_C = h \times 8.6$ GHz, and $E_L = h \times 5650$ GHz. In this very frustrated regime, the lowest level of the CPT crosses the lowest level of the LC resonator with approaching the charge degeneracy point $n_g = 0.5$; this results in the avoided level crossing. (b) Enlargement of the theoretical curves in the region of avoided level crossing (black curves), together with the dependence of the color-coded microwave amplitude S_{21} on the microwave frequency f and n_g measured for one of the tested CPTs at $\phi_B = 0.97\pi$. The dependence of $S_{21}(f)$ at the charge degeneracy point $n_g = 0.5$ is shown in (c).

diagonalization of the Hamiltonian (8) leads to the theoretical predictions that can be compared with the data.

Our experimental situation corresponds to $E_c \sim 2\hbar\omega_0$ and $E_J \sim 4\hbar\omega_0$. In the absence of frustrations, the frequency of the lowest CPT level is very high: $\omega_p = \sqrt{8E_cE_J} \sim 10\omega_0$. The frequency of the lowest CPT level decreases as the magnetic field frustrates the Josephson coupling and/or with approaching the charge degeneracy ($n_g = 0.5$). Figure 3(a) shows three low-energy levels of the system "CPT + LC resonator" with the parameters typical for our experiment. Note that for the studied circuits, only the combined effect of flux- and charge-induced frustrations brings the frequency of the first device level below that of the LC resonator, otherwise the device resonance frequency significantly exceeds that of the LC resonator even at full flux frustration (e.g., $\omega = 2E_c > 4\omega_0$ at $n_g = 0$).

IV. EXPERIMENTAL RESULTS AND DISCUSSION

Below, we present the measurements of the amplitude S_{21} of the transmitted microwaves (unless otherwise specified) at the base temperature $T = 20$ mK. Most of the data [with the exception of the data in Figs. 3(b), 3(c), and 6] are shown for only one representative device. The resonant dependence of S_{21} on the microwave frequency $f = \omega_2/2\pi$, measured for this device at $\phi_B = 0$ and $n_g = 0$, is shown in the inset to Fig. 4. The resonance frequency depends periodically on n_g and ϕ_B; for example, the dependence $f_r(n_g,\phi_B)$ measured at $n_g = 0$ is shown in Fig. 4. The period in charge is $\Delta n_g = 2e$ at the base temperature (see Fig. 5); it changes from $2e$ to e at higher temperatures (>300 mK) due to the presence of thermally excited quasiparticles (data not shown). Note that the total time of acquisition for the data shown in Fig. 3(b) was approximately 20 minutes; over longer time intervals, the periodicity of $f_r(n_g,\phi_B)$ might be disrupted by the motion of nonequilibrium quasiparticles to/from the CPT island (the so-called "quasiparticle poisoning"[18]) or other types of charge fluctuations.[21] The high stability of the charge on the CPT island indicates that (a) the combination of a larger superconducting gap of the CPT island and its relatively large charging energy protects the CPT from quasiparticle poisoning, and (b) the double-wall rf-tight sample box shields the device from stray high-energy photons. The microwave photon energy $E_{\rm ph} \approx h \times 7$ GHz is insufficiently large to excite the CPT at $n_g = 0$: indeed, according to our simulations, the lowest excitation frequency for this device exceeds 30 GHz even at full flux frustration ($\Phi/\Phi_0 = 0.5$). In this case, the variation of the resonance frequency f_r with magnetic flux reflects the ϕ_B dependence of the CPT impedance in its ground state.

The dependencies of the resonance frequency on n_g are illustrated by Figs. 5(a)–5(e), where the color-coded microwave amplitude S_{21} is plotted versus f and n_g for several values of the magnetic flux in the device loop. The black

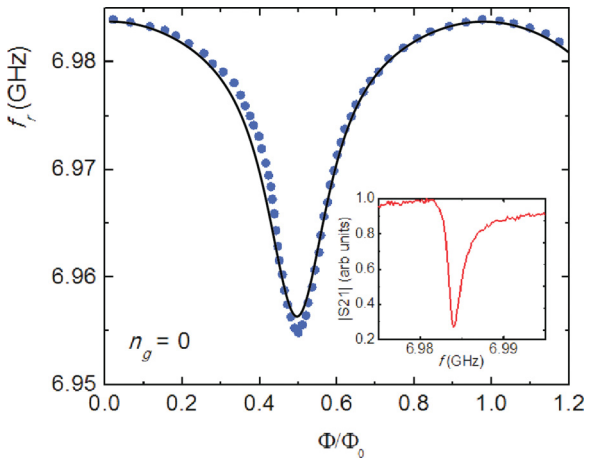

FIG. 4. (Color online) Dependence of the resonance frequency $f_r(n_g = 0,\phi_B)$ on the magnetic flux Φ, which controls the phase difference across the CPT, $\phi_B = 2\pi\Phi/\Phi_0$. The solid curve shows the numerical simulation with the fitting parameters discussed in the text. The inset shows the dependence of the microwave amplitude S_{21} on the frequency near the resonance at $\phi_B = 0$ and $n_g = 0$.

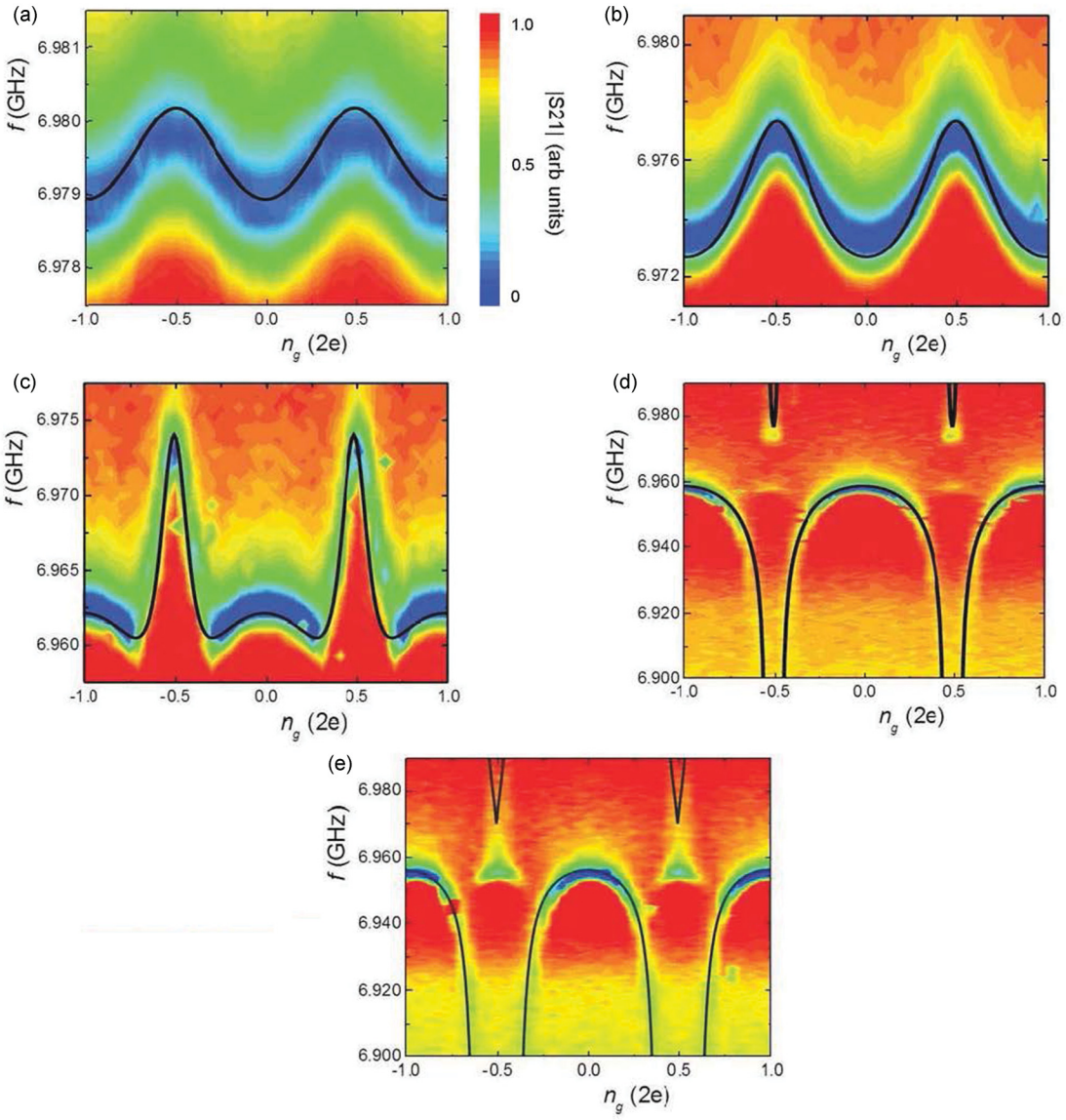

FIG. 5. (Color online) The color-coded plots of the microwave amplitude $|S_{21}|$ vs the microwave frequency f and the charge n_g induced on the CPT island by the gate voltage. The phase difference across the CPT was controlled by the magnetic flux Φ in the device loop: (a) $\Phi/\Phi_0 = 0.29$, (b) $\Phi/\Phi_0 = 0.375$, (c) $\Phi/\Phi_0 = 0.45$, (d) $\Phi/\Phi_0 = 0.47$, and (e) $\Phi/\Phi_0 = 0.5$. The solid curves show the numerical simulations with the fitting parameters discussed in the text.

curves in Fig. 5 show the results of fitting the experimental data with our numerical simulations. All these curves were generated with the same set of fitting parameters: $E_C = h \times 16$ GHz, $E_J = h \times 32$ GHz, and $E_L = h \times 5720$ GHz (note that not only the amplitude of the resonance frequency modulation, but also the absolute values of f_r are predetermined by these parameters). The fitting procedure is very sensitive to the choice of these parameters: we believe that they are determined with an accuracy better than 10%. The extracted charging energy coincides (within 5% accuracy) with an estimate of E_C based on the junction area, the specific geometrical capacitance for Al tunnel junctions (50 fF/μm^2, see, e.g., Ref. 22) and the electronic capacitance of Josephson junctions, $C_e = 3/16(R_Q/R)e^2/\Delta$ (0.3 fF at $R = 3$ kΩ).[23,24] The Josephson energy estimated on the basis of the Ambegaokar-Baratoff relationship[25] using the normal-state resistance of a test junction fabricated on the same chip is approximately 40% greater than the fit value of E_J.

Generally, one expects that Josephson circuits can be accurately described by the Hamiltonian consisting of Josephson and charging energies [cf. Eq. (2)] only if all energy scales are much smaller than Δ. For frequencies $\omega \sim \Delta/\hbar$, the Josephson coupling becomes frequency dependent, whilst at higher frequencies $\omega > 2\Delta/\hbar$ it is purely dissipative. This should significantly affect the quantum processes with energies $\omega \sim \Delta/\hbar$ and even more so: the virtual processes involving higher energy excitations (such as charge fluctuations on the CPT island by values greater than $2e$). Away from full frustration, the energy of the CPT excited state is of the order of Josephson plasma frequency $\approx$3.2 K, which is comparable

to Δ. Thus the excellent agreement between the experimental data and numerical modeling, observed over the whole range of n_g and ϕ_B, is quite surprising.

It is worth noting that the circuit modeling based on the numerical diagonalization of the circuit Hamiltonian is essential for fitting the data for devices with $E_J/E_C \sim 2$. For example, the analytical solution for the Josephson inductance in the CPT ground state, calculated within the two-level approximation [cf. Eq. (4) in Ref. 9], overestimates the amplitude of the $f_r(n_g)$ dependence at small flux frustrations by almost an order of magnitude. The latter solution provides more accurate fitting of the experiment at larger frustrations [$\phi_B \sim (0.8–9)\pi$], but becomes inadequate again at $\phi_B > 0.94\pi$ when the avoided level crossing is observed.

The evolution of these dependencies reflects the modification of the CPT spectrum with n_g and ϕ_B. For a small phase difference ϕ_B [see Figs. 5(a) and 5(b)], the lowest CPT excitation frequency well exceeds the microwave frequency (which is close to the resonance frequency of the LC resonator), and the CPT remains in its ground state for all n_g including the charge degeneracy point ($n_g = 0.5$). In this regime, the dependencies $S_{21}(f,n_g)$ mostly reflect the variations of the CPT impedance with n_g in the CPT ground state. With an increase of frustrations, the shape of the $f_r(n_g)$ curves becomes more complicated. Our numerical simulations show that the entanglement of the device and resonator states becomes important when the lowest CPT level approaches the lowest resonator level at $n_g = 0.5$ even if it has not crossed it yet [cf. Fig. 5(c) at $\phi_B = 0.9\pi$]. Two comments are in order here. First, although the $f_r(n_g)$ dependence in Fig. 5(c) qualitatively resembles the solution within the two-level approximation, the quantitative agreement even at this strong frustration is absent. Second, the $f_r(n_g)$ dependence similar to the one shown in Fig. 5(c) was observed at full frustration in experiment[17] for much lower resonance frequencies of the tank circuit. The authors of work[17] interpreted their result as the evidence for nonequilibrium quasiparticles. In contrast, we were able to quantitatively describe the data by numerically solving Hamiltonians (8) and (12) that do not involve quasiparticles.

Finally, with further approach to full frustration [$\phi_B \geqslant 0.94\pi$, Figs. 5(d) and 5(e)], the CPT excitation frequency becomes smaller than the resonance frequency of the LC resonator, and the shape of the $f_r(n_g)$ dependences abruptly changes: they are strongly affected by the avoided level crossing. The $S_{21}(f,n_g)$ plots in this regime consist of two sets of curves. The lower set of curves corresponds to the lowest energy level of the combined system "CPT + LC resonator" (this level coincides with the CPT lowest level when approaching the charge degeneracy points, i.e., far away from the resonance frequency of the LC resonator). The upper set of curves corresponds to the first excited level of the system "CPT + LC resonator": when approaching the charge degeneracy point, this level descends from higher energies to its lowest position at $n_g = 0.5$. The visibility of the upper set of curves depends on the proximity between the CPT and LC resonator levels. Indeed, if the energy of the CPT resonance at $n_g = 0.5$ is much lower than the first LC resonator level, the upper-curve "cone" is very sharp, and the corresponding microwave resonance is smeared even for small deviations of n_g from 0.5 [this case is illustrated by Figs. 5(d) and 5(e)]. On the other hand, the "cone" becomes broader when the intersecting CPT and LC resonator levels are close to one another; in this case, illustrated by Fig. 1(b), we were able to follow the upper set of curves over the frequency range of approximately15 MHz.

For both devices, whose dependencies $S_{21}(f,n_g)$ are shown in Figs. 3 and 5, we observed a double-resonance structure at full frustration and charge degeneracy [see Figs. 3(b), 3(c) and 5(e)]. The second (lower-frequency) resonance appears as a "shadow" of the resonance observed at $n_g = 0$. The appearance of this resonance, much weaker than that at $n_g = 0$, implies that there are fluctuations of the island offset charge $\pm e$ that are fast at the measuring time scale approximately 0.1 s. These fluctuations change the effective n_g from 0.5 to 0. We attribute these fluctuations to the nonequilibrium quasiparticles moving between the CPT island and the leads. At $n_g = 0.5$, the energy of a quasiparticle on the island exceeds the energy of quasiparticles in the leads by $\delta\Delta - (1/2)E_C$. Here, $\delta\Delta$ is the difference between superconducting gaps in the island and the leads due to the difference in the thicknesses of these Al films; we estimate $\delta\Delta$ to be approximately $k_B \times 0.3K$. In our devices, the probability of these fluctuations is small (the amplitude of the $n_g = 0$ resonance is much greater than that of its "shadow" at $n_g = 0.5$), which suggests that the quantity $\delta\Delta - (1/2)E_C$ in our devices is positive (albeit small).

To evaluate the charge sensitivity δQ of the CPT we used the method developed in Ref. 26. In addition to applying a dc gate voltage to tune the CPT to an optimal operating point, a sinusoidal signal at frequency 2 MHz was applied to the gate electrode; its amplitude corresponded to the charge variations of $0.07e_{\rm rms}$ on the CPT island. Due to the amplitude modulation of the transmitted probe signal, two satellite peaks separated by 2 MHz from the main probe-frequency

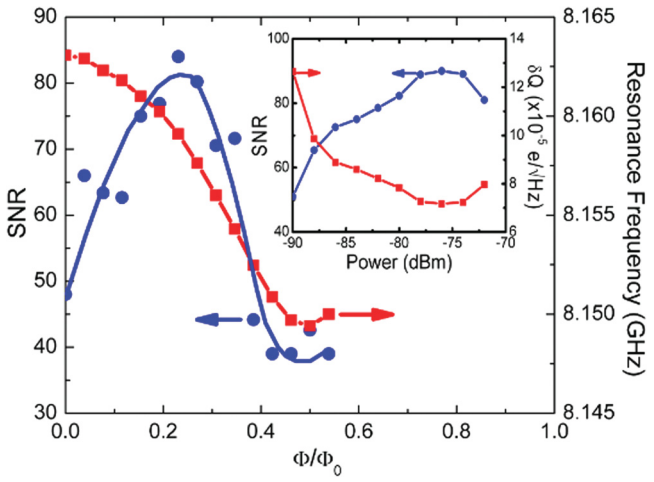

FIG. 6. (Color online) Dependence of the signal-to-noise ratio (blue circles) and the resonance frequency of the coupled CPT + LC resonator $f_r(n_g = 0)$ (red squares) on the magnetic flux Φ measured at a microwave power of −80 dBm. A 2-MHz signal with amplitude corresponding to $0.07e_{\rm rms}$ charge variations on the CPT island was applied to the gate of the CPT. Solid curves are guides for the eye. The inset shows the signal-to-noise ratio (blue circles) and charge sensitivity (red squares) as a function of microwave probe power.

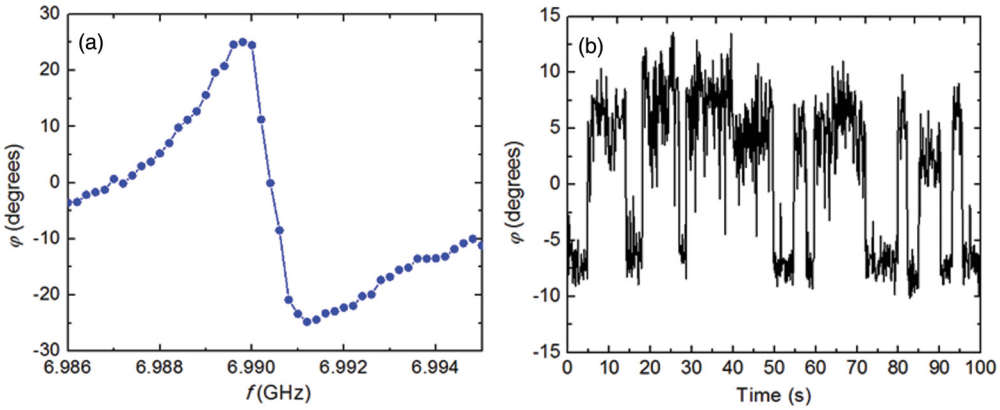

FIG. 7. (Color online) (a) Dependence of the phase φ of the transmitted microwaves on the microwave frequency near the resonance of the "CPT + LC resonator" circuit. The CPT is in a strongly frustrated regime ($\phi_B = \pi$, $n_g = 0.17$), when an avoided crossing between the CPT and LC resonator levels is observed. The measurement time for each experimental point is 24 ms. (b) The microwave phase measured with the same averaging time (24 ms/point) at a fixed microwave frequency $f = 6.9905$ GHz over a time period of 100 s. The full range of phases from -15° to $+15^\circ$ corresponds to the offset charge variation by $0.05e$.

peak appeared on the transmitted microwave spectrum. The probe signal frequency was set at or near the CPT + LC resonance. The signal-to-noise ratio (SNR) of the satellite peaks obtained with a resolution bandwidth of 122 Hz is shown as a function of the magnetic flux in Fig. 6. The SNR maximum is observed when the CPT excitation frequency approaches the LC resonance; this regime corresponds to the n_g dependence of the CPT + LC resonance shown in Fig. 5(a). Though the avoided crossing between the lowest CPT and LC resonator levels results in a larger amplitude of the $f_r(n_g)$ variations near full frustration [see Figs. 5(c)–5(e)], the SNR drops in this regime because of a significant broadening of the resonances. We observed that, similar to the results of Ref. 26, the SNR reaches its maximum at a probe microwave power of –76 dBm (the inset in Fig. 6), and drops at higher powers where the rf-amplitude exceeds the gap voltage of the CPT. The maximum charge sensitivity in our setup is $\delta Q = 7 \times 10^{-5} e/\sqrt{\text{Hz}}$; it is limited by the preamplifier noise and thus can be further improved by using a quantum-limited preamplifier.

The CPT can be used to probe charge fluctuations in its local environment. Figure 7(b) shows the time dependence of the phase φ of transmitted microwaves when the microwave frequency is tuned to the resonance of the "CPT + LC resonator" circuit. The telegraph noise was measured at full flux frustration ($\phi_B = \pi$) when an avoided crossing between the CPT and LC-resonator levels was observed, but relatively far from the charge degeneracy point ($n_g = 0.17$). The amplitude of the observed telegraph noise corresponds to the charge fluctuations $\Delta q \approx 0.05e$ due to coupling of the CPT island to a single charge fluctuator in its environment. The time resolution of these measurements is limited by the response time of the LC resonator, approximately 1 μs.

V. CONCLUSIONS

We have performed a detailed analysis of the microwave response of Cooper pair transistors with $E_J/E_C \sim 1.5$–3 coupled to an LC resonator as a function of the magnetic flux and the gate voltage. Away from the full frustration in flux and charge the excitation frequencies of the Cooper pair transistor are far away from the LC resonator frequency. In this regime, the modulation of the resonance frequency of the coupled system induced by the CPT can be described in terms of the modulation of the effective CPT inductance. Close to the full frustration the excitation level of the Cooper pair transistor approaches and eventually crosses the LC resonator excitation level; this results in a complex dependence of resonance frequency of the coupled system on the flux and gate voltage. In all regimes, the dependence of the resonance frequency of the system "CPT + LC resonator" on n_g and ϕ is very well described by the results of the numerical diagonalization of the full Hamiltonian of the coupled system. High sensitivity of the resonance frequency to n_g provides a tool to measure charge fluctuations in the environment with high accuracy and short-time resolution.

ACKNOWLEDGMENTS

We would like to thank J. Aumentado and V. Manucharyan for helpful discussions. We acknowledge the support from the DARPA (under grant HR0011-09-1-0009), ARO (W911NF-09-1-0395), and NSF (NIRT ECS-0608842).

[1]D. Averin and K. Likharev, in *Mesoscopic Phenomena in Solids*, edited by B. Altshuler, P. Lee, and R. A. Webb (North-Holland, Amsterdam, 1991), p. 173.

[2]J. Aumentado, in *The Handbook of Nanophysics* (Taylor and Francis, New York, 2010), p. 779.

[3]M. A. Sillanpaa, L. Roschier, and P. J. Hakonen, Phys. Rev. Lett. **93**, 066805 (2004).

[4]T. Duty, G. Johansson, K. Bladh, D. Gunnarsson, C. Wilson, and P. Delsing, Phys. Rev. Lett. **95**, 206807 (2005).

[5]O. Naaman and J. Aumentado, Phys. Rev. B **73**, 172504 (2006).
[6]Y. Nakamura, Y. Pashkin, and J. Tsai, Nature (London) **398**, 786 (1999).
[7]D. Vion, A. Aassime, A. Cottet, P. Joyez, H. Pothier, C. Urbina, D. Esteve, and M. Devoret, Science **296**, 886 (2002).
[8]A. Wallraff, D. I. Schuster, A. Blais, L. Frunzio, J. Majer, M. H. Devoret, S. M. Girvin, and R. J. Schoelkopf, Phys. Rev. Lett. **95**, 060501 (2005).
[9]A. Paila, D. Gunnarsson, J. Sarkar, M. A. Sillanpaa, and P. J. Hakonen, Phys. Rev. B **80**, 144520 (2009).
[10]A. Widom, G. Megaloudis, T. Clark, J. Mutton, R. Prance, and H. Prance, J. Low Temp. Phys. **57**, 651 (1984).
[11]D. Averin, A. Zorin, and K. Likharev, Sov. Phys. JETP **61**, 407 (1985).
[12]M. A. Sillanpaa, T. Lehtinen, A. Paila, Y. Makhlin, L. Roschier, and P. J. Hakonen, Phys. Rev. Lett. **95**, 206806 (2005).
[13]B. Doucot and L. B. Ioffe, Phys. Rev. B **76**, 214507 (2007).
[14]S. Gladchenko, D. Olaya, E. Dupont-Ferrier, B. Doucot, L. B. Ioffe, and M. E. Gershenson, Nat. Phys. **5**, 48 (2009).
[15]A. B. Zorin, Phys. Rev. Lett. **86**, 3388 (2001).
[16]D. Born, V. I. Shnyrkov, W. Krech, T. Wagner, E. Il'ichev, M. Grajcar, U. Hubner, and H.-G. Meyer, Phys. Rev. B **70**, 180501 (2004).
[17]J. Konemann, H. Zangerle, B. Mackrodt, R. Dolata, and A. B. Zorin, Phys. Rev. B **76**, 134507 (2007).
[18]J. Aumentado, M. W. Keller, J. M. Martinis, and M. H. Devoret, Phys. Rev. Lett. **92**, 066802 (2004).
[19]V. Manucharyan, J. Koch, L. Glazman, and M. Devoret, Science **326**, 113 (2009).
[20]R. Barends, J. Wenner, M. Lenander, Y. Chen, R. C. Bialczak, J. Kelly, E. Lucero, P. O Malley, M. Mariantoni, D. Sank *et al.*, Appl. Phys. Lett. **99**, 113507 (2011).
[21]L. Faoro and L. B. Ioffe, Phys. Rev. Lett. **96**, 047001 (2006).
[22]P. Delsing, C. Chen, D. Haviland, Y. Harada, and T. Claeson, Phys. Rev. B **50**, 3959 (1994).
[23]A. Larkin and Y. Ovchinnikov, Phys. Rev. B **28**, 6281 (1983).
[24]U. Eckern, G. Schon, and V. Ambegaokar, Phys. Rev. B **30**, 6419 (1984).
[25]M. Tinkham, *Introduction to Superconductivity* (McGraw-Hill Book Co, New York, 1996).
[26]A. Aassime, G. Johansson, G. Wendin, R. J. Schoelkopf, and P. Delsing, Phys. Rev. Lett. **86**, 3376 (2001).